Machining Oxide Thin Films with an Atomic Force Microscope: Pattern and Object Formation on the Nanometer Scale

Yun Kim; Charles M. Lieber

Science, New Series, Vol. 257, No. 5068 (Jul. 17, 1992), 375-377.

Stable URL:
http://links.jstor.org/sici?sici=0036-8075%2819920717%293%3A257%3A5068%3C375%3AMOTFWA%3E2.0.CO%3B2-B

The decade of the 1980s was the warmest on record, 0.4°C warmer on average than any other decade. Of the ten warmest years in the record, five have occurred since 1981. Although this temperature signal and the associated rise in steric height are not implausibly above the background level of decadal variability, the trend observed in the past 42 years is a matter for both strong concern and interest.

REFERENCES AND NOTES

1. B. C. Douglas, *J. Geophys. Res.* **96**, 6981 (1991).
2. W. R. Peltier and A. M. Tushingham, *Science* **244**, 806 (1989).
3. National Research Council Panel on Sea Level Change, *Sea Level Change*, R. Revelle, chairman (National Academy Press, Washington, DC, 1990).
4. F. P. Bretherton, R. E. Davis, C. B. Fandry, *Deep-Sea Res.* 23, 559 (1976).
5. Steric height is the integral over pressure of specific volume anomaly, here from 500 dbar (equivalent to a depth of about 500 m) to the ocean surface. For example, the effect of warming the upper 100 dbar of the ocean, say from 15° to 16°C at a salinity of 34 practical salinity unit (psu), is to increase the thickness of that layer of water by 2.2 cm. In order to increase the thickness by the same fraction by salinity change, a decrease in salinity from 34 to about 33.7 psu would be required. The equation of state for seawater is given by: *Technical Papers in Marine Science 36* (Unesco, Paris, 1981).
6. A. Bakun, *Science* **247**, 198 (1990).
7. A. M. Tushingham and W. R. Peltier, *J. Geophys. Res.* **96**, 4497 (1991).
8. W. E. Carter *et al.*, *Woods Hole Oceanographic Institute Technical Report WHOI-89-31* (1989).
9. R. E. Thomson and S. Tabata, *Mar. Geod.* **11**, 103 (1987).
10. D. Roemmich, in *Sea Level Change*, National Research Council Panel on Sea Level Change, R. Revelle, chairman (National Academy Press, Washington, DC, 1990), chap. 13.
11. D. Roemmich and C. Wunsch, *Nature* **307**, 447 (1984).
12. N. Bindoff and J. Church, *ibid.* **357**, 59 (1992).

13. The many scientists and technical support personnel responsible for the existence and high quality of the CalCOFI data are gratefully acknowledged. This study was supported by the Scripps National Institution of Oceanography's Marine Life Research Group and by National Science Foundation grant 90-04230 (World Ocean Circulation Experiment).

9 March 1992; accepted 6 May 1992

Machining Oxide Thin Films with an Atomic Force Microscope: Pattern and Object Formation on the Nanometer Scale

Yun Kim and Charles M. Lieber*

An atomic force microscope (AFM) has been used to machine complex patterns and to form free structural objects in thin layers of MoO_3 grown on the surface of MoS_2. The AFM tip can pattern lines with ≤10-nanometer resolution and then image the resulting structure without perturbation by controlling the applied load. Distinct MoO_3 structures can also be defined by AFM machining, and furthermore these objects can be manipulated on the MoS_2 substrate surface with the AFM tip. These results suggest application to nanometer-scale diffraction gratings, high-resolution lithography masks, and possibly the assembly of nanostructures with novel properties.

The ability to manipulate matter and to assemble novel structures on the atomic to nanometer scale is currently a goal of many researchers in the physical and engineering sciences (*1–15*). One attractive strategy for achieving this goal is to use scanning probe microscopes, such as the scanning tunneling microscope (STM) or AFM, to move atoms or clusters of atoms directly into a desired configuration. For example, the STM has been used to remove single atoms from surfaces (*2*, *3*), to position atoms on a surface (*4*, *5*), and to create an atomic switch (*6*). On a nanometer scale the STM has also been used to create structures by field-assisted diffusion (*5*, *7*), to develop organic resists (*8*), to expose passivated semiconductor surfaces (*9*), and to deposit gold islands on gold surfaces (*10*). Most recently the STM has been used to induce the dissociation of a single molecule on a silicon surface (*11*). In contrast, there are few examples of controlled, high-resolution manipulation with the AFM. Several groups have shown that direct contact (repulsive mode) imaging of soft organic layers under sufficiently high loads can lead to orientational ordering or removal or both of this organic layer from the area scanned by the AFM tip (*12*, *13*). The length scale or resolution of these modifications typically has been ≥100 nm. In addition, AFM tip-induced wear of transition-metal dichalcogenide materials has been reported (*14*, *15*) on a ≥50-nm scale. The results from these AFM studies are promising; however, the resolution and control of the surface features produced by the AFM are poor compared to structures created with the STM.

We believe that the materials used in these previous AFM studies have significantly limited the attainable resolution and selectivity. Hence, we have sought to explore the limits of direct surface manipulation with the AFM using a novel material system that consists of a thin (<50 Å) metal oxide film (MoO_3) on the surface of MoS_2. In comparison to previous studies, this system has several important features: (i) the thin MoO_3 film is rigid and nondeformable, in contrast to organic layers; (ii) MoO_3 can be selectively machined or imaged depending on the applied load of the AFM cantilever; and (iii) the MoS_2 substrate, which is a good lubricant, functions as an integral stop layer that automatically fixes the depth of the structures. We used this system to demonstrate controlled pattern development with ≤10-nm resolution and complex machining of movable objects that have nanometer dimensions. The generalization of these results to other materials and their potential applications to nanotechnologies are discussed.

Thin crystallites of α-MoO_3 were grown on the surface of single-crystal 2H-MoS_2 by thermal oxidation by using purified O_2 at 480°C for 5 to 10 min. The MoO_3 layers were identified by transmission electron diffraction, x-ray photoemission spectroscopy, and atomic-resolution AFM images (*16*). These studies have shown that α-MoO_3 (space group *Pbnm*) grows with the b-axis (13.848 Å) perpendicular to the MoS_2 substrate surface. For the above oxidation conditions, MoO_3 crystallites one to three unit cells thick (one unit cell = b-axis = 13.85 Å) and 200 to 500 nm on edge are formed. Additional details of the MoS_2 oxidation process and the characterization of the MoO_3 thin crystal layers will be discussed in detail elsewhere (*16*). All of the AFM experiments were carried out with a modified commercial instrument (Nanoscope, Digital Instruments, Santa Barbara, California). Si_3N_4 cantilever and tips (force constant $k \approx 0.38$ N/m) were used for imaging and modification. In addition, the AFM experiments were carried out in a nitrogen-filled glove box equipped with a purification system that reduced the concentrations of oxygen and water to less than 5 and 2 ppm, respectively. This environment enables us to obtain the reproducible conditions needed for controlled surface modification (*17*)

A typical image of a MoO_3 crystallite formed after thermal oxidation of MoS_2 at 480°C is shown in Fig. 1A. The MoO_3 has a thickness of ~15 Å (corresponding to one unit cell along b) and occupies most of the central portion of this 500 nm by 500 nm image. Atomic-resolution images confirm this structural assignment: the a-c plane of

Department of Chemistry and Division of Applied Sciences, Harvard University, Cambridge, MA 02138.

*To whom correspondence should be addressed.

MoO_3 has orthorhombic symmetry, a = 3.97 Å and c = 3.70 Å, and the (0001) surface of MoS_2 has hexagonal symmetry, a = 3.16 Å (insets, Fig. 1A). In addition, the MoO_3 and MoS_2 surfaces are stable to repetitive scanning when the imaging force is $\leq 10^{-8}$ N.

However, when the applied force is increased to $\geq 5 \times 10^{-8}$ N, we find that the MoO_3 surface can be machined in a controlled manner with high resolution. In Fig. 1B we show an image of the same area of the surface acquired after machining a line in the MoO_3 thin film. The line has a resolution of ~10 nm at the MoO_3 surface and 5 nm at its bottom and is approximately one unit cell deep (*18*). These features are shown clearly in a three-dimensional line scan image and cross-sectional view (Fig. 1C). From this latter data it is also clear that the structure is microscopically very smooth. In addition, continued scanning does not lead to features deeper than the thickness of the MoO_3 thin layer. The MoS_2 substrate, which is a good solid lubricant, functions as a self-limiting stop in this modification process. We believe that the mechanism by which this structure is created is simply tip-induced wear of the MoO_3 surface. Our experimental data strongly support this mechanistic assignment because we find that the rate of structure formation is proportional to the applied load ($\geq 5 \times 10^{-8}$ N) and to the scan rate (35 to 470 nm/s). Furthermore, the cross section of the line (Fig. 1C) matches the Si_3N_4 tip shape determined by electron microscopy. In analogy to macroscopic processes, this tip-induced wear can be termed "nanomachining."

An important criteria for any reliable and potentially practical machining process is that the cutting tool (in our case the AFM tip) undergoes minimal wear compared to the substrate. In order to examine this issue and to determine the complexity and reproducibility of the patterns that can be created, we have nanomachined a series of lines to pattern "HU" in the MoO_3 (Fig. 1, D to F). Importantly, we find that the resolution does not degrade during this series of nanomachining operations. In addition, the resulting HU structure is stable during continuous imaging with loads $\leq 10^{-8}$ N. Our work thus demonstrates that it is possible to create complex, durable, and high-resolution patterns in the MoO_3 thin layers. There are several applications that one can envision with this system. It is possible with our technology to fabricate nanometer-resolution diffraction gratings. The length of the grating lines would not be limited to the size of the crystallites produced by oxidation because it is possible to deposit uniform crystalline films of MoO_3 on MoS_2 by laser ablation (*19*). It also will

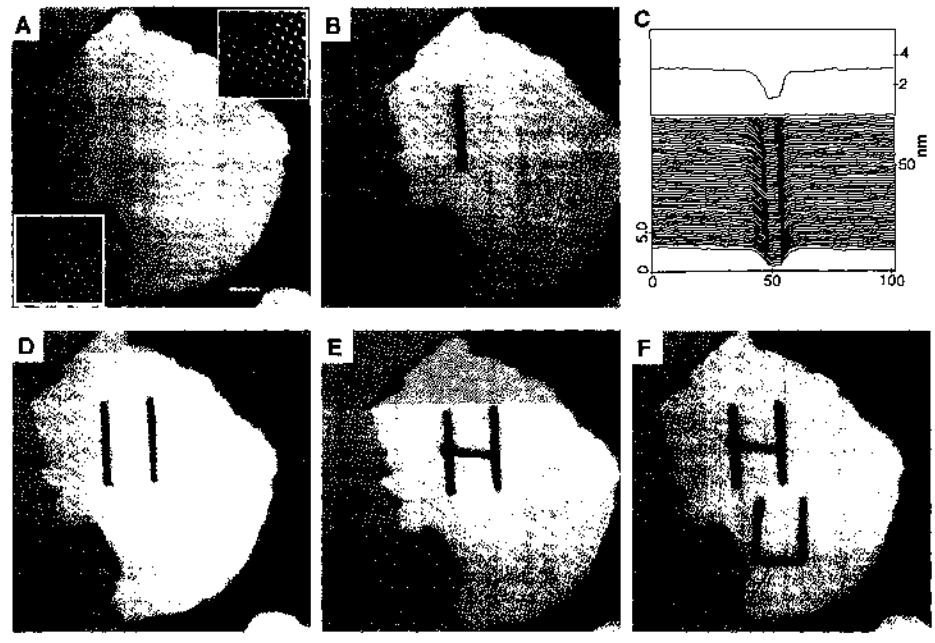

Fig. 1. A series of 500 nm by 500 nm AFM images that depict the patterning of a MoO_3 crystallite with the letters "HU." All of the images were recorded with an applied load of 1×10^{-8} N. (**A**) A 500 nm by 500 nm image of MoO_3 grown on the surface of a MoS_2 single crystal. The irregular shaped object occupying the central portion of this image is the MoO_3 crystallite, and the surrounding regions correspond to the MoS_2 substrate. The insets shown in the lower and upper corners of this figure are atomic resolution images (3.5 nm by 3.5 nm) recorded on the MoS_2 and MoO_3 areas, respectively; the lattice parameters and symmetry of these images confirm the material assignment (see text). (**B**) A line machined in the MoO_3 crystal with an applied load of 5×10^{-8} N. (**C**) Zoomed view of this structure rendered as a three-dimensional line scan. A single scan across the line is also shown in the upper portion of this image. (**D** to **F**) A series of 500 nm by 500 nm images illustrating sequential machining of the MoO_3 crystallite to define the HU pattern. The white bar in (A) represents 50 nm and also defines the length scale for (B), (D), (E), and (F).

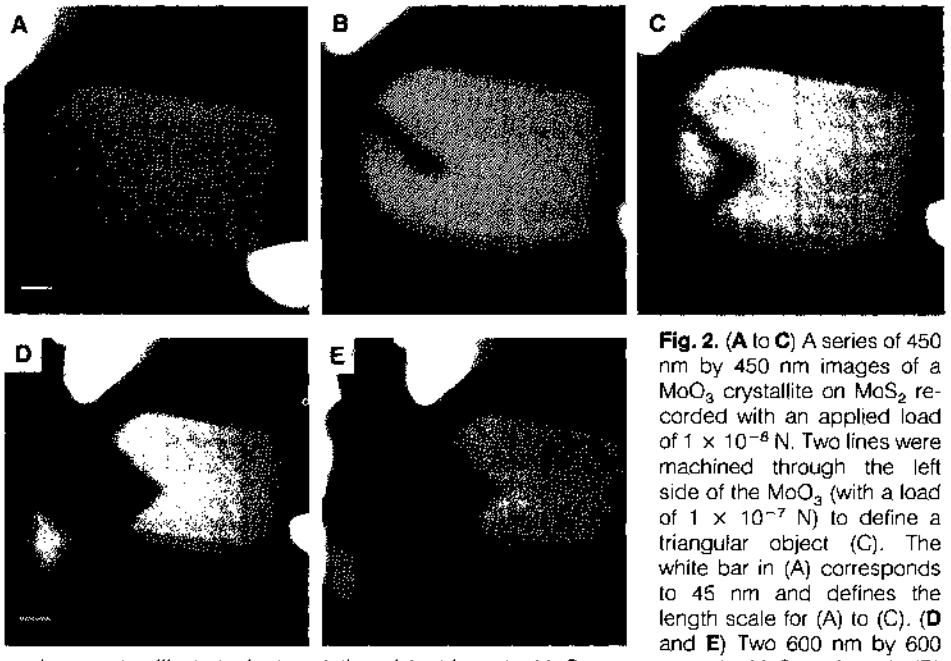

Fig. 2. (**A** to **C**) A series of 450 nm by 450 nm images of a MoO_3 crystallite on MoS_2 recorded with an applied load of 1×10^{-8} N. Two lines were machined through the left side of the MoO_3 (with a load of 1×10^{-7} N) to define a triangular object (C). The white bar in (A) corresponds to 45 nm and defines the length scale for (A) to (C). (**D** and **E**) Two 600 nm by 600 nm images that illustrate the translation of the triangular MoO_3 structure on the MoS_2 surface. In (D) the triangle has been moved ~100 nm from its position in (C). It was translated an additional 100 nm before recording image (E). Images (D) and (E) were recorded with an applied load of 1×10^{-8} N; translation was carried out with a higher load, 1×10^{-7} N. The white bar in (D) corresponds to 60 nm and defines the length scale for (D) and (E).

be interesting to consider the use of patterned MoO_3 films as masks for high-resolution x-ray lithography. In a more general sense, it should be possible to use these ideas for nanomachining other inorganic thin layers, such as SiO_x on Si, when the substrate (for example, Si) wears at a rate significantly slower than the inorganic coating (for example, SiO_x) (*20*).

We can also go beyond the level of simply patterning a surface and make distinct objects that can be manipulated and in principle incorporated into complex nanostructures. The basis for this new idea is the fact that the MoO_3 crystallites are not strongly bound to the underlying MoS_2 substrate; therefore, it is possible to separate nanomachined MoO_3 objects from the MoS_2 surface. This concept is demonstrated in Fig. 2. In this series of AFM images we first define a triangle at the edge of a MoO_3 crystallite (Fig. 2, A to C). The line pattern defining the triangle was machined with a force of 1×10^{-7} N (*21*). The most remarkable feature of this series of images is that the triangular structure patterned at the edge of the MoO_3 can be separated from the original crystallite by scanning across the entire crystal with a force of $\sim 1 \times 10^{-7}$ N (Fig. 2D). In Fig. 2D the triangular object was moved ~100 nm after a single high-load scan. We can further manipulate the triangular MoO_3 object on the MoS_2 with this procedure and show a second ~100-nm translation step in Fig. 2E. Importantly, these translation steps can be imaged without perturbation by using low loads ($\leq 10^{-8}$ N). Hence, we are not only able to nanomachine free objects, but we can also translate and observe these objects on the MoS_2 surface with an AFM tip. The objects we create and manipulate with the AFM are several orders of magnitude smaller than those currently produced by micromachining techniques (*22*). For future applications it is important to note that the electronic properties of MoO_3 can be readily varied from insulating through metallic by doping, and that MoO_3 and related metal oxides exhibit photochromism. Because it should be possible to lift these small objects electrostatically with the tip (in addition to translating them), it is interesting to speculate whether one can assemble nanostructures with novel electrical and optical properties by using these techniques.

REFERENCES AND NOTES

1. For recent reviews, see *Science* **254**, 1300 (1991); P. Ball and L. Garwin, *Nature* **355**, 761 (1992).
2. I.-W. Lyo and Ph. Avouris, *Science* **253**, 173 (1991).
3. D. Cleary, *New Sci.* **129**, 31 (1991); J. L. Huang, Y. E. Sung, C. M. Lieber, unpublished results.
4. D. M. Eigler and E. D. Schweizer, *Nature* **344**, 524 (1990).
5. J. A. Stroscio and D. M. Eigler, *Science* **254**, 1319 (1991).
6. D. M. Eigler, C. P. Lutz, W. E. Rudge, *Nature* **352**, 600 (1991).
7. L. J. Whitman, J. A. Stroscio, R. A. Dragoset, R. J. Celotta, *Science* **251**, 1206 (1991).
8. C. R. K. Marrian, E. A. Dobisz, R. J. Cotton, *J. Vac. Sci. Technol. A* **8**, 3563 (1990); E. A. Dobisz and C. R. K. Marrian, *Appl. Phys. Lett.* **58**, 2526 (1991).
9. J. A. Dagata *et al.*, *Appl. Phys. Lett.* **56**, 2001 (1990).
10. H. J. Mamin, S. Chiang, H. Birk, P. H. Guethner, D. Rugar, *J. Vac. Sci. Technol. B* **9**, 1398 (1991).
11. G. Dujardin, R. E. Walkup, Ph. Avouris, *Science* **255**, 1232 (1992).
12. G. S. Blackman, C. M. Mate, M. R. Philpott, *Vacuum* **41**, 1283 (1990).
13. O. M. Leung and M. C. Goh, *Science* **255**, 64 (1992).
14. Y. Kim, J.-L. Huang, C. M. Lieber, *Appl. Phys. Lett.* **59**, 3404 (1991).
15. E. Delawski and B. A. Parkinson, *J. Am. Chem. Soc.* **114**, 1661 (1992).
16. Y. Kim and C. M. Lieber, in preparation.
17. In air, the MoO_3 and MoS_2 surfaces wear in an uncontrolled manner. A strong adhesive interaction between the tip and sample, which is due to adsorbates, is believed to be responsible in large part for this observed wear. Within the glove box, however, the MoS_2 surface does not wear on our experimental time scale, and the wear of the MoO_3 can be controlled by the applied load.
18. Lines with similar widths but only 3 Å deep have been formed previously in the metallic oxide $Rb_{0.3}MoO_3$ by an unknown process with an STM: E. Garfunkel *et al.*, *Science* **246**, 99 (1989).
19. C. Niu and C. M. Lieber, unpublished results.
20. A stable tip is required to obtain reproducible nanomachining. For other oxide systems the Si_3N_4 tips may not be sufficiently robust; however, cantilevers with diamond tips should be applicable to a wide range of materials.
21. The line resolution at the surface of the MoO_3 is lower than in Fig. 1 because this crystallite is three times thicker (42 Å) than the one unit cell–thick MoO_3 layer patterned with HU.
22. K. D. Wise and K. Najafi, *Science* **254**, 1335 (1991).

23. C.M.L. acknowledges support of this work by the Air Force Office of Scientific Research and the David and Lucile Packard Foundation. Y.K. dedicates this work to S.-J. Kim on the occasion of his 60th birthday.

3 April 1992; accepted 11 May 1992

Recovery from Hemophilia B Leyden: An Androgen-Responsive Element in the Factor IX Promoter

Merlin Crossley,* Michael Ludwig, Kathryn M. Stowell, Piet De Vos, Klaus Olek, George G. Brownlee†

One form of the inherited, X-linked, bleeding disorder, hemophilia B, resolves after puberty. Mutations at −20 and −26 in the clotting factor IX promoter impair transcription by disrupting the binding site for the liver-enriched transcription factor LF-A1/HNF4. The −26 but not the −20 mutation also disrupts an androgen-responsive element, which overlaps the LF-A1/HNF4 site. This explains the improvement seen in patients with the −20 mutation and the failure of the −26 patient to recover.

Patients with Hemophilia B Leyden present in childhood with severe bleeding symptoms and <1% of the normal amounts of plasma factor IX. After puberty, the clinical symptoms improve gradually and plasma factor IX concentrations rise to 60% of normal. The first known patient had a T to A mutation at −20 in the factor IX promoter (*1*). Other Leyden-like patients, have point mutations at nucleotides −6, +6, +8, or +13 (*2*). Here we study a new patient who failed to improve after puberty and suggest an explanation for the clinical improvement.

The patient, Hemophilia B Brandenburg, had a G to C mutation at −26 in the promoter region (*3*). Like the classical Leyden patients, he had <1% normal amounts of factor IX clotting activity before puberty, but unlike them, his factor IX clotting remained low and there was no clinical recovery (*3*). To test whether this −26 mutation and the −20 mutation (*1*) impaired transcription from the factor IX pro-

M. Crossley, K. M. Stowell, G. G. Brownlee, Chemical Pathology Unit, Sir William Dunn School of Pathology, University of Oxford, South Parks Road, Oxford OX1 3RE, United Kingdom.
M. Ludwig, Institute of Experimental Hematology and Blood Transfusion, University of Bonn, Sigmund-Freud-Strasse 25, 5300 Bonn 1, Germany.
P. De Vos, Laboratory of Experimental Medicine and Endocrinology (LEGENDO), Catholic University, Leuven, Belgium.
K. Olek, Institute of Clinical Biochemistry, University of Bonn, Sigmund-Freud-Strasse 25, 5300 Bonn 1, Germany.

*Present address: Childrens Hospital, and Department of Pediatrics, Harvard Medical School, Boston, MA 02115.
†To whom correspondence should be addressed.

Table 1. CAT activity in HepG2 cells comparing normal, Brandenburg, and Leyden promoters. Each construct contained −189 to +21 of the factor IX promoter fused to the CAT gene in the promoterless vector pCAT00 (*4*). Mean and standard errors of three independent experiments are shown.

Promoter construct	Relative CAT activity (%)
Normal	100 ± 4.6
Brandenburg (−26 G to C)	2.9 ± 0.8
Leyden (−20 T to A)	3.8 ± 0.5
pCAT00	2.7 ± 1.1